Responses to the Comments of the Anonymous Referee #2

We appreciate the further comments and suggestions from this reviewer. Our point-by-point responses to the reviewer's comments are as follows (the reviewer's comments are marked in Italic font).

Comments:

This paper examines the impacts of biomass burning aerosols on convective systems over the northern Sumatra and the western Borneo in the Maritime Continent based on based on longterm WRF-Chem simulations. The authors have made efforts to address reviewers' comments and improve the manuscript. The improvements make the paper much clearer and its conclusions better defended. I have a few suggestions and questions outlined below, which I believe can be addressed with minor revisions prior to publication.

1. Line 221-224: Why not define the threshold first and then select the representative case for analysis?

As we mentioned in the manuscript, the selected cases are chosen randomly from different fire periods of the two study regions. We did not know what should be a proper criterion to distinguish weak from strong convections among these samples beforehand. It was actually not our initial intention as well because the selected samples might not represent the overall statistics – notice that the weak versus strong is rather relative. After we analyzed all cases, we found that biomass burning aerosols impact on relative weak and strong convections differently. Thus, we set 3 mm 3hr^{-1} as the threshold to distinguish weak and strong convections for the following discussion in the manuscript.

2. Section 3.2: The precipitation and hydrometeor properties are analyzed. How is the convective intensity? e.g., updrafts.

Indeed, discussions in Sect. 3.2 are about the impacts of biomass burning aerosols on microphysical features and precipitation. The discussion of convective intensity is mainly in Sect. 3.4.

3. Line 335-341: This is only the cold-phase invigoration effect (Rosenfeld 2008). For tropical regions with high humidity, small size aerosols may also show warm-phase invigoration due to additional activation (Fan et al, 2018).

We thank the reviewer's suggestion. We added the Rosenfeld et al. (2008) for the cold-phase invigoration effect and "For tropical regions with high humidity, additional aerosols may also lead to the warm-phase invigoration due to the consequent enhancement in total condensed water quantity and thus latent heat release (Wang, 2005; Fan et al., 2018)" in the revised manuscript.

4.Line 480: biomass burning activities may include the released heat, aerosols and water

vapor. Since you only discuss the effect of biomass burning aerosol, I would suggest to change "activities" to "aerosols".

Modified as the reviewer suggested.

5. Fig 11: What are 20LST and 02LST showing? The peak of difference? It is better to show a time series of sea breeze and land breeze change and link with the near surface temperature change.

We appreciate the comment of the reviewer. We have added the following sentences in the manuscript: "Figure 11 illustrates the sea breeze increase in FFBB during the daytime (20 LST) and the land breeze decrease in FFBB during the nighttime (2 LST). Twenty LST and 2 LST are chosen here because of the peak of difference".

The time series is hard to see the transition of sea breeze and land breeze change so that we present the peak of difference in the figure. Adding surface temperature change may make the figure too busy to read. For time series change of temperature and other parameters, the readers can get the information from Fig. 12.

The Impacts of Biomass Burning Activities on Convective Systems in the Maritime Continent

Hsiang-He Lee[1][*][@] and Chien Wang[1,2][**]

[1] Center for Environmental Sensing and Modeling, Singapore-MIT Alliance for Research and Technology, Singapore

[2] Center for Global Change Science, Massachusetts Institute of Technology, Cambridge, MA, U.S.A.

[*]Now at Atmospheric, Earth, and Energy Division, Lawrence Livermore National Laboratory, Livermore, CA, U.S.A.

[**]Now at Laboratoire d'Aerologie/CNRS/University of Toulouse, Toulouse, France

July 2019

[@]Corresponding author address: Dr. Hsiang-He Lee, 7000 East Avenue, Livermore, CA, 94550, U.S.A.

E-mail: lee1061@llnl.gov

Abstract

Convective precipitation associated with Sumatra squall lines and diurnal rainfall over Borneo is an important weather feature of the Maritime Continent in Southeast Asia. Over the past few decades, biomass burning activities have been widespread during summertime over this region, producing massive fire aerosols. These additional aerosols brought to the atmosphere, besides influencing local radiation budget through directly scattering and absorbing sunlight, can also act as cloud condensation nuclei or ice nuclei to alter convective clouds and precipitation in the Maritime Continent via the so-called aerosol indirect effects. Based on four-month simulations with or without biomass burning aerosols conducted using the Weather Research and Forecasting model with chemistry package (WRF-Chem), we have investigated the aerosol-cloud interactions associated with the biomass burning aerosols in the Maritime Continent. Results from selected cases of convective events have shown significant impacts of fire aerosols specifically on the weak convections by increasing the quantities of hydrometeors and rainfall in both Sumatra and Borneo regions. Statistical analysis over the fire season also suggests that fire aerosols have impacts on the nocturnal convections associated with the local anticyclonic circulation in the western Borneo and then weakened the nocturnal rainfall intensity by about 9%. Such an effect is likely come from the near surface heating by absorbing aerosols emitted from fires that could weaken land breezes and thus the convergence of anticyclonic circulation.

2

1 Introduction

Biomass burning in Southeast Asia has become a serious environmental and societal issue in the past decade due to its impact on local economy, air quality, and public health (Miettinen et al., 2011; Kunii et al., 2002; Frankenberg et al., 2005; Crippa et al., 2016; Lee et al., 2018).   Abundant aerosols emitted from such fires not only cause environmental issues but also affect regional weather and climate through the direct and indirect effects of biomass burning aerosols (Grandey et al., 2016; Hodzic and Duvel, 2017; Jeong and Wang, 2010; Ramanathan and Carmichael, 2008; Taylor, 2010; Tosca et al., 2013).   Carbonaceous compounds such as black carbon (BC) in biomass burning aerosols can reduce sunlight through both absorption and scattering to warm the atmosphere while cool the Earth's surface (Fujii et al., 2014; Andreae and Gelencsér, 2006; Satheesh and Ramanathan, 2000; Ramanathan et al., 2001).   Besides these direct effects, biomass burning aerosols can act as cloud condensation nuclei or ice nuclei to alter cloud microphysical structures and thus cloud radiation. Such "indirect effects" of these aerosols on the climate are even more complicated due to various cloud and meteorological conditions (Sekiguchi et al., 2003; Lin et al., 2013; Wu et al., 2013; Grandey et al., 2016; Ramanathan et al., 2001; Wang, 2004).

For the Maritime Continent in Southeast Asia, convective precipitation associated with the so-called Sumatra squall lines (SSL) and diurnal rainfall over Borneo is an important weather feature (Lo and Orton, 2016; Ichikawa and Yasunari, 2006; Koh and Teo, 2009; Yi and Lim, 2006; Wu et al., 2009). Convections of SSL are initially formed in the northwestern side of Sumatra by the prevailing sea breezes from Indian Ocean and the Sumatran mountain range, then propagate over the Malacca Strait affecting the Malay

3

79   Peninsula. Lo and Orton (2016) analyzed 22-year (1988 to 2009) ground-based Doppler

80   radar data and identified a total of 1337 squall lines in Singapore. They found that these

81   events with the diurnal cycle of rainfall most occur during either the summer monsoon

82   season (June-September) or the inter-monsoon periods (April-May and October-

83   November). Singapore, for example, experiences typically about 6~7 squall lines per

84   month during these periods. Oki and Musiake (1994) analyzed the seasonal and diurnal

85   cycles of precipitation using rain gauge data and showed that large-scale low-level winds

86   are a critical modulating factor in the diurnal cycle the convective rainfall over Borneo

87   besides the general reason of land-sea contrast behind convective rainfall in the Maritime

88   Continent. Furthermore, Ichikawa and Yasunari (2006) used five years Tropical Rainfall

89   Measuring Mission (TRMM) precipitation radar (PR) data to investigate the role of the

90   low-level prevailing wind in modulating the diurnal cycle of rainfall over Borneo. They

91   found that the diurnal cycle is associated with intraseasonal variability in the large-scale

92   circulation pattern, with regimes associated with either low-level easterlies or westerlies

93   over the island.

94   Interestingly, frequent biomass burning activities coincide with vigorous convective

95   systems in the Maritime Continent, especially during the summer monsoon season (June-

96   September), and could thus produce aerosols to affect convections in the region.

97   Rosenfeld (1999) analyzed TRMM data and hypothesized that abundant biomass burning

98   aerosols could practically shut off warm rain processes in tropical convective clouds.

99   Compared to the adjacent tropical clouds in the cleaner air, clouds encountered with

100   smokes could grow to higher altitudes with rain suppressed, hypothetically due to the

101   reduction of coalescence efficiency of smaller cloud drops into raindrops. Recently,

4

102 using Weather Research and Forecasting model with Chemistry (WRF-Chem), Ge et al.

103 (2014) have studied the direct and semi-direct radiative effects of biomass burning

104 aerosols over the Maritime Continent and found the radiative effect of biomass burning

105 aerosols could alter planetary boundary layer (PBL) height, local winds (including sea

106 breeze), and cloud cover. However, relative coarse resolution (27 km) adopted in their

107 simulation would not be able to reveal more details about how biomass burning aerosols

108 affect convective clouds through modifying cloud microphysics processes. Whereas,

109 Hodzic and Duvel (2017) have conducted a 40-day simulation using WRF-Chem with a

110 convection-permitting scale (4 km) to study the fire aerosol-convection interaction during

111 boreal summer in 2009 near the central Borneo mountainous region. Their result

112 suggests that modifications of the cloud microphysics by biomass burning aerosols could

113 reduce shallow precipitation in the afternoon and lead to a warm PBL anomaly at sunset,

114 all lead to an enforcement of deep convection at night. However, they have also

115 indicated that the radiative processes of moderately absorbing aerosols tend to reduce

116 deep convection over most regions due to local surface cooling and atmosphere warming

117 that increase the static stability, hence suggesting the complexity of the interaction of

118 biomass burning aerosols and convective clouds in the Maritime Continent.

119   In this study, we aim to examine and quantify the impacts of biomass burning

120 aerosols on convective systems over two targeted regions for analyses: the northern

121 Sumatra and the western Borneo in the Maritime Continent. Our focus is on not only the

122 change of hydrometeors in the convective clouds but also the change of rainfall amount

123 and intensity in these regions. We firstly describe methodologies adopted in the study,

124 followed by the results and findings from our numerical simulations over the Maritime

5

125 Continent. We have selected three cases in each study region to perform detail analyses.

126 In addition, statistical analyses covering the entire modeled fire season for each of these

127 two regions have also been performed to provide more generalized pictures about the

128 effects of fire aerosol on convection. The last section summarizes and concludes our

129 work.

130 2 Methodology

131 2.1 Model and emission inventories

132   In order to simulate trace gases and particulates interactively with the meteorological

133 fields, the Weather Research and Forecasting model coupled with a chemistry module

134 (WRF-Chem, see Grell et al. (2005)) version 3.6.1 is used in this study. Within WRF-

135 Chem, the Regional Acid Deposition Model, version 2 (RADM2) photochemical

136 mechanism (Stockwell et al., 1997) coupled with the Modal Aerosol Dynamics Model for

137 Europe (MADE) as well as the Secondary Organic Aerosol Model (SORGAM)

138 (Ackermann et al., 1998; Schell et al., 2001) are included to simulate atmospheric

139 chemistry and anthropogenic aerosol evolutions. MADE/SORGAM uses a modal

140 approach to represent the aerosol size distribution and predicts mass and number

141 concentrations of three aerosol modes (Aiken, accumulation, and coarse).

142   To resolve the convective system in the Maritime Continent in our simulations, two

143 model domains with two-way nesting are designed. Here, Domain 1 (431 × 141 grid

144 cells) has a resolution of 25 km, while Domain 2 (561 × 591 grid cells) has a resolution

145 of 5 km (Fig. 1). Specifically, Domain 1 is positioned to include the tropical Indian

146 Ocean on its west half in order to capture the path of Madden-Julian Oscillation (MJO),

6

147 and in the meantime to have a northern boundary constrained within 23°N in latitude to

148 avoid potential numerical instability from the terrain of Tibetan Plateau. Domain 2 with

149 a finer resolution is positioned to cover the mainland Southeast Asia as well as the islands

150 of Sumatra and Borneo.

151   The National Center for Environment Prediction FiNaL (NCEP-FNL) reanalysis

152 data (National Centers for Environmental Prediction, 2000) are used to provide initial and

153 boundary meteorological conditions, and to perform four-dimensional data assimilation

154 (FDDA) to nudge model temperature, water vapor, and zonal and meridional wind speeds

155 above the planetary boundary layer (PBL) for Domain 1. The time frequency of nudging

156 is every 6 hrs. The Mellor-Yamada-Nakanishi-Niino level 2.5 (MYNN) (Nakanishi and

157 Niino, 2009) is chosen as the scheme for planetary boundary layer in this study. Other

158 physics schemes adopted in the simulations include Morrison two-moment microphysics

159 scheme (Morrison et al., 2009), RRTMG longwave and shortwave radiation schemes

160 (Mlawer et al., 1997; Iacono et al., 2008), Unified Noah land-surface scheme (Tewari et

161 al., 2004), and Grell-Freitas ensemble cumulus scheme (Grell and Freitas, 2014) (for

162 Domain 1 only). Owing to the main purpose of this study to reveal fire aerosol-

163 convection interaction through modeling a large quantity of convective systems

164 continually over a relatively long period, and the computational resource available to us

165 as well, we have adopted a 5 km horizontal resolution which excluding cumulus

166 parameterization scheme. Previous studies have shown that WRF model with a similar

167 resolution without convection parameterization can still capture many critical

168 characteristics of deep convection (Wagner et al., 2018). Our model evaluation,

7

169 especially through the comparison of modeled results with sounding profiles, has

170 demonstrated the same.

171   WRF-Chem needs emissions for gaseous and particulate precursors to drive its

172 simulations. For this purpose, we have used the Regional Emission inventory in ASia

173 (REAS) version 2.1 (Kurokawa et al., 2013). REAS includes emissions of most primary

174 air pollutants and greenhouse gases, covering each month from 2000 to 2008. In

175 addition, the Fire INventory from U.S. National Center for Atmospheric Research

176 (NCAR) version 1.5 (FINNv1.5) (Wiedinmyer et al., 2011) is also used in the study to

177 provide biomass burning emissions. FINNv1.5 classifies burnings of extratropical forest,

178 tropical forest (including peatland), savanna, and grassland. Fire heat fluxes for four

179 different types of fire are prescribed in WRF-Chem to calculate the plume height (rf.

180 Table 1 in Freitas et al. (2007)). For peatland fire, we have set its heat flux as 4.4 kW m^{-}

181 ^{2}, which is the same as that of savanna burning and differs from that of the tropical forest

182 burning in 30 kW m^{-2}. The modified the plume rise algorithm in WRF-Chem to

183 specifically improve the representation of tropical peat fire has been described in Lee et

184 al. (2017). It is worth indicating that the heat flux from biomass burning is not

185 incorporated in thermodynamic equation of current WRF-Chem model. Note that the

186 current fire emission inventories could underestimate near surface fire aerosol

187 concentration by ignoring some of the characteristics of smoldering burning as well (Shi

188 et al., 2019).

189 The default chemical profiles of several species in the lateral boundary condition are

190 higher than their background concentrations in our study region and thus equivalent to

191 provide additional aerosol sources from boundaries. To prevent this, we have set NO,

8

192   NO_2, SO_2, and all primary aerosol levels to zero at the lateral boundaries of Domain 1.

193   We have also adjusted the ozone profile used for lateral boundary condition based on the

194   World Meteorological Organization (WMO) Global Atmosphere Watch (GAW) station

195   in Bukit Kototabang, Indonesia (Lee et al., 2019).

2.2   Numerical experiment design

197   Two numerical simulations, both included anthropogenic emissions (mainly fossil

198   fuel emissions) while either with and without the biomass burning emissions (labeled as

199   FFBB and FF, respectively), have been conducted to investigate the impacts of biomass

200   burning aerosols on convective systems in the Maritime Continent through both direct

201   and indirect effects. Our study focuses on the fire season from June to September of

202   2008. Therefore, the simulations start from 1 May of 2008 and last for five months. The

203   first month is used as a spin-up period. Among the years with available emission data,

204   both emission amount of biomass burning and total precipitation in 2008 approximate

205   their ensemble mean or represent an average condition (Fig. S1). Nevertheless,

206   interannual variation of biomass burning emissions alongside precipitation in the studies

207   regions do exist (Lee et al., 2017; Lee et al., 2018), and the influence of such variation on

208   the effects of fire aerosol on convection should be addressed in future studies.

2.3   Analysis methods

210   The primary target of this study is the convective systems associated with Sumatra

211   squall lines and diurnal rainfall over Borneo. Thus, our analyses mainly focus on the

212   convections over two specific regions: the Sumatra region (r1 in Fig. 1) and the Borneo

213   region (r2 in Fig. 1). The area coverage of the Sumatra region (r1) is from 97° to 103° E

9

214 in longitude and 0° to 6° N in latitude, while the area coverage of the Borneo region (r2)

215 is from 109° to 115° E in longitude and 1° S to 5° N in latitude.

216   To examine the impacts of fire aerosols on cloud formation and rainfall intensity as

217 well as amount, we have selected three convective systems each for the two focused

218 regions to perform an in-depth case study. We first trace the path of individual

219 convections and focus the analyses on the specific area of each of these convective

220 systems to identify the impacts of fire aerosols. Table 1 shows the selected cases in the

221 Sumatra region (r1) and the Borneo region (r2). The selected cases are chosen randomly

222 from different fire periods of the two study regions. We did not set any criteria initially

223 when we chose these cases. After we analyzed all cases, 3 mm 3hr^{-1} was set as the

224 threshold to distinguish weak and strong convections.

225   The consequent analyses are then focused on the fire-season-wise statistics of

226 convections for each study region. Table 2 and Fig. S2 show the fire periods in the two

227 study regions. There are total of 54 convective systems simulated during the fire periods

228 in the Sumatra region (r1) and 35 convective systems in the Borneo region (r2).

229   The statistical quantities used in this study follows Wang (2005) to estimate the

230 mean value over a specific region (e.g., r1 or r2). The cloud area mean quantities are

231 defined as a function of output time step (t) by the following equation:

232
$$\bar{c}^{area}(t) = \frac{1}{N(t)}\sum_{\substack{q>qmin\\n>nmin}} c(x,y,z,t). \tag{1}$$

233 Here c is a given quantity (e.g., cloud water mass). Eq. (1) only applies to the grid points

234 where both the mass concentration q and number concentration n of a hydrometeor

235 exceed their given minima. The total number of these grid points at a given output time

236 step t is represented by $N(t)$. The cloud area mean quantities are used to present the

10

237   average quantities of a given variable at a given output time step. Note that the cloud

238   area mean quantities only apply to hydrometeors. For rainfall, the analyzed quantities are

239   spatial averages over a specific area of the convective system for case study or over the

240   entire study region for longer-term statistic estimate.

241   **3   Results**

242   **3.1 Model evaluation**

243   **3.1.1 Precipitation**

244   The satellite-retrieved precipitation of the Tropical Rainfall Measuring Mission

245   (TRMM) 3B42 3hrly (V7) dataset (Huffman et al., 2007) is used in this study to evaluate

246   simulated rainfall. Figure 2a and 2b show the Hovmöller plots of daily TRMM and

247   FFBB precipitation from 1 June 2008 to 30 September 2008, respectively. Compared to

248   the satellite-retrieved data, the model has captured all the major rainfall events in the two

249   analysis regions (Fig. 3).   In addition, because of its higher spatial resolution than

250   TRMM, the model produces more light rain events. Nevertheless, as indicated in our

251   previous study (Lee et al., 2017), a wet bias of the model is evident and mainly comes

252   from water vapor nudging in data assimilation (FDDA). As a result, the daily average

253   rainfall in FFBB over the Sumatra region (r1) is 11.05±5.90 mm day^{-1} from 1 June 2008

254   to 30 September 2008, higher than that of 7.21±5.54 mm day^{-1} derived from TRMM

255   retrieval. The wet bias also exists in the modeling results in the Borneo region (r2),

256   where daily average rainfall there is 15.40±8.49 mm day^{-1} in FFBB and only 9.56±7.20

257   mm day^{-1} in TRMM. For the simulated rainfall in FFBB, the temporal correlation with

258   TRMM is 0.44 in the Sumatra region (r1) and 0.64 in the Borneo region (r2).

3.1.2 Aerosol optical depth (AOD)

Because of limited ground-based observational data of aerosols, we use Aerosol Optical Depth (AOD) from the level-3 Moderate Resolution Imaging Spectroradiometer (MODIS) gridded atmosphere monthly global joint product (MOD08_M3; http://dx.doi.org/10.5067/MODIS/MOD08_M3.061) to evaluate modeled aerosol spatial distribution and relative concentration. Figure 4a shows MODIS monthly AOD in Southeast Asia in September 2008. High AOD occurs in the southern part of Sumatra and the southwestern part of Borneo. Compared to the MODIS retrieval, the modeled AOD in FFBB has similar spatial distribution but a higher value (Fig. 4b). It is because a high spatiotemporal resolution in our simulation enables the model to capture episodic fire events better. In contrast, FF simulation produces much lower AOD values than those of MODIS and FFBB, thus suggesting biomass burning aerosols make a substantial fraction in atmospheric AOD during burning seasons.

3.1.3 Sounding profiles

We have used multiple weather sounding profiles measured in Bintulu Airport, Malaysia (113.03° E, 3.20° N), provided by University of Wyoming (http://weather.uwyo.edu/upperair/sounding.html). An example for detailed summary is a case at 12 UTC on 22 September 2008 (Fig. 5a). This sounding provides information of atmospheric state (e.g., vertical distributions of pressure, temperature, wind speed, wind direction, and humidity) coinciding with one of our selected case study (r2c3) of diurnal convective rainfall in Borneo. Compared to the observed sounding data, the FFBB simulation has produced similar temperature and wind profiles and well captured

12

281 the low-level and high-level wind speeds and wind directions (Fig. 5a versus 5b). It also

282 well predicts several key indexes of convection: temperature and pressure of the Lifted

283 Condensation Level (LCL) simulated in FFBB are 296.2 K and 955 hPa, respectively,

284 which are close to the values of 296.2 K in temperature and 960.7 hPa in pressure derived

285 from the observed sounding data. The model predicts 3049 J of Convective Available

286 Potential Energy (CAPE), while 2031 J of CAPE is estimated in the observed sounding

287 data. Besides this 22 September 2008 case, the model has also captured major features of

288 observed profiles for all the other cases selected in our analyses shown in Fig. S3~S7.

289 ### 3.1.4 Cloud vertical structure

290 The Cloud-Aerosol Lidar and Infrared Pathfinder Satellite Observation (CALIPSO)

291 provides information of the vertical structure of clouds on its path around the globe

292 (https://www-calipso.larc.nasa.gov/products/lidar/browse_images/production/), including

293 that of one of our cases (r2c3) of diurnal convective rainfall in Borneo on 22 September,

294 2008 (Fig. 6a). For this case, CALIPSO shows the vertical structure of a convective

295 system over Borneo along with high $PM_{2.5}$ concentration near the surface (yellowish

296 color near the surface), implying a potential impact of biomass burning aerosols on

297 convective clouds. It can be seen that the FFBB simulations well captures the vertical

298 structure of convective clouds as well as the near-surface aerosol layers, including their

299 vertical extension (Fig. 6c versus 6a). With the comparison of FF simulation, we are able

300 to identify the biomass burning origin of these aerosols near the surface. It is worth to

301 indicate that we have compared more than 50 modeled convections during the fire season

302 and within the simulation domains. However, the others captured by CALIPSO are

13

303 either not among the selected cases or are mostly out of our analyzed domains, so we did

304 not have further discussion here.

3.2 Analyses of selected cases in two study regions

3.2.1 The Sumatra region (r1)

307 The three selected cases in r1 or the Sumatra region (r1c1, r1c2 and r1c3) all

308 occurred in the afternoon (2 PM or 5 PM local time) and lasted less than 24 hours (Table

309 1). The sounding profile of three cases show quite similar to the environmental profiles

310 (Fig. S3~S5). Most fire aerosols in this study region were initially emitted from the

311 central and south Sumatra then transported along with southwesterly winds to encounter

312 convections in the northern Sumatra. Compared to the result of FF, $PM_{2.5}$ concentration

313 in FFBB can be 6~12 times higher in the Sumatra region (r1) in these selected cases (Fig.

314 7).

315 Aerosols from biomass burning in FFBB add 2~3 times more cloud droplet number

316 concentration and 8~20% higher cloud water mass compared to the results in FF (Table

317 2). The mean radius of cloud droplets in FFBB is about 6~7 μm, clearly smaller than that

318 in FF (10~11 μm). Smaller cloud droplet in FFBB reduces the efficiency of

319 autoconversion, and further decreases rain water mass and raindrop number

320 concentration. Hence, raindrop number concentration in FFBB is 40~50% lower than

321 that in FF among our selected cases in r1 (Table 3). However, besides autoconversion,

322 rain water mass is also affected by other microphysics processes. Larger raindrops

323 combining with smaller cloud droplets in FFBB can enhance the efficiency of cloud

324 droplet collection by rain and thus increase rain water mass but cause no change to the

14

325 number of raindrops, possibly compensating the decrease of rain water mass resulted

326 from a lowered autoconversion. Overall, rain water mass decreases 15% in the case of

327 r1c2 and 10% in the case of r1c3, respectively. Compared to the cases of r1c2 and r1c3,

328 the case of r1c1 is a relatively weak convective system based on a threshold of ~3 mm

329 $3hr^{-1}$ of the averaged rainfall in FF (Table 4). After introducing fire aerosols, the mass

330 concentration of snow and graupel in this case increases 62% and 48%, respectively.

331 Melting snow and graupel in the lower atmosphere results in a significant increase of rain

332 water mass concentration by 49%. Thus, total hydrometeor mass is increased by 36% in

333 FFBB from that in FF. Our result is consistent with that of Lin et al. (2006), which

334 suggested that biomass burning aerosols could invigorate convection and then increase

335 precipitation based on satellite observations. The aerosol invigoration effect is referred to

336 such a hypothetic process that increasing number of smaller cloud droplets due to higher

337 aerosol concentration would reduce the efficiency of raindrop formation from self-

338 collection among cloud droplets, and thus further slowdown the loss of these small

339 droplets from being collected by larger raindrops and allow more of them reach high

340 altitudes, where they would eventually collected by ice particles through riming, causing

341 release of latent heat to enhance updraft (Rosenfeld et al., 2008). For tropical regions

342 with high humidity, additional aerosols may also lead to the warm-phase invigoration due

343 to the consequent enhancement in total condensed water quantity and thus latent heat

344 release (Wang, 2005; Fan et al., 2018). Note that the "aerosol-aware" microphysics

345 scheme in WRF-Chem only applies to the warm cloud process (Morrison et al., 2005;

346 Morrison et al., 2009); therefore, ice nucleation is parameterized of ambiance temperature

347 only regardless of the aerosol concentration. In our model configuration, fire aerosol can

15

Hsiang-He Lee 1/16/2020 9:04 PM
Deleted: .

349 still affect ice process, however, through CCN effect rather than serving directly as ice
350 nuclei.

351   In the FF simulations, the convective system in the case of r1c2 and r1c3 is stronger
352 than the system in the case of r1c1, and the average rainfall of r1c2 and r1c3 is also
353 higher than the rainfall of r1c1 (Table 4). Adding fire aerosols in FFBB does not
354 substantially change the average rainfall in r1c2 and r1c3 (+3% and -8%, respectively;
355 Table 4). However, in the relatively weak convective system of r1c1, adding fire
356 aerosols significantly increases the mean rainfall amount by 106% (1.33 ± 0.47 mm $3hr^{-1}$
357 in FF versus 2.74 ± 1.21 mm $3hr^{-1}$ in FFBB).

3.2.2 The Borneo region (r2)

359   The three selected cases in r2 (r2c1, r2c2, and r2c3) also occurred during the summer
360 monsoon season when active biomass burning events existed in the west Borneo. In
361 these cases, fire aerosols were transported to the north and northeast by the southeasterly
362 and southwesterly winds. Because of the proximity of fire emissions, the $PM_{2.5}$
363 concentration in FFBB can be 24 times higher than that in FF in the Borneo region (r2) in
364 these selected cases (Fig. 7).

365   The modeled results demonstrate the substantial impacts of fire aerosols on both
366 ambient aerosol concentration and cloud droplet number concentration. $PM_{2.5}$
367 concentration in FFBB is drastically higher than that in FF with the highest increase
368 appears in the case of r2c1 at 4940%, more than doubled the values of r2c2 (2402%) and
369 r2c3 (2422%). The increase in cloud droplet number concentration in the case of r2c1
370 (703%) is also substantially higher than those in r2c2 (337%) and r2c3 (409%) (Table 2).

16

371   The mean radius of cloud droplets in FFBB is about 6~7 μm, which is significantly

372   smaller than that in FF (10~11 μm). The mean cloud droplet radii in FF and FFBB in r2

373   are similar to the results in r1. On the other hand, the increase of cloud water mass due to

374   fire aerosols is not so dramatic in all these cases, only about 8%~27% higher than that in

375   the FF simulations (Table 3). As discussed above, rain number concentration in FFBB

376   over the Borneo region (r2) is lower than that in FF, similar to the cases in r1, likely due

377   to the low efficiency of autoconversion induced by the presence of a large quantity of

378   smaller cloud droplets. Rain water mass of FFBB in the r2c1 case is decreased by about

379   6% due to fire aerosols, which is similar to the results in the r1c2 and r1c3 cases over the

380   Sumatra region (Table 3). However, interestingly, rain water and snow mass are both

381   increased in FFBB by 64% and 69% in r2c2 and by 19% and 60% in r2c3, respectively

382   (Table 3). The cases of r2c2 and r2c3 are relatively weak convective systems, similar to

383   the case of r1c1. Again, it is based on based on a threshold of ~3 mm 3hr^{-1} of the

384   averaged rainfall in FF (Table 4). Our results show that fire aerosols have substantial

385   impacts on cold cloud processes in the weak convective systems.   Overall, total

386   hydrometeor mass concentration in FFBB have increased 47% in r2c2 and 13% in r2c3.

387   The changes of rainfall amount due to fire aerosols in r2 are similar to the cases in r1.

388   For the strong convection case of r2c1, adding fire aerosols in the FFBB simulation

389   decreases the total rainfall amount by 18%. However, in the weak convection cases of

390   r2c2 and r2c3, adding fire aerosols would double the rainfall amount (Table 4).

391   Compared to the results in FF, rainfall intensity is persistently higher in FFBB during the

392   convection life cycle in those weak convection cases. Nighttime rainfall intensity in

393   FFBB, especially, is much higher than the rainfall intensity in FF. Therefore, as shown

17

394   by our results, fire aerosols appear to have more substantial impacts on the quantities of

395   hydrometeors and rainfall of the weak convection cases in both Sumatra region (r1) and

396   Borneo region (r2).

397   Our results show that fire aerosols tend to invigorate weak convection but suppress

398   deep convection in both Sumatra region (r1) and Borneo region (r2). As mentioned

399   before, increasing the number of smaller cloud droplets due to higher aerosol

400   concentration resulted from fire would reduce the efficiency of raindrop formation

401   through the warm-rain processes, thus allowing more cloud droplets reach high altitudes

402   to be eventually collected by ice particles through riming, causing release of latent heat to

403   invigorate updraft while enhancing precipitation through melting of fallen ice particles

404   (Wang, 2005). These processes appear to be more effective to weak convections than

405   deep convections and were in fact well-simulated in the former cases. The results are

406   also consistent with some previous observation-based studies (Jiang et al., 2018; Zhao et

407   al., 2018). Jiang et al. (2018) and Zhao et al. (2018) both concluded that an increase of

408   fire aerosols generally reduces cloud optical thickness of deep convection while Zhao et

409   al. (2018) further showed that fire aerosols tend to invigorate weak convection for small-

410   to-moderate aerosol loadings.

411   ## 3.3 Fire-season statistics of convections in two study regions

412   Statistics covering the entire simulated fire season (~4 months) for each study region

413   have been derived to provide trend/tendency information regarding several aspects of the

414   impact of fire aerosols on convections. In our simulations, $PM_{2.5}$ concentration in FF

415   during the fire periods, which can be regarded as the background value for FFBB

18

416 simulation before adding fire aerosols, is 1.36 ± 0.19 µg m^{-3} in r1 and 0.56 ± 0.09 µg m^{-3} in

417 r2. In comparison, PM$_{2.5}$ concentration in FFBB is 11.37 ± 10.41 µg m^{-3} in r1 and

418 10.07 ± 7.73 µg m^{-3} in r2. Note that unlike in some other studies where the control

419 simulations use constant aerosol concentrations, fire aerosol concentrations in our

420 simulations can vary in responses to changes in fire emissions, or aerosol removal by rain

421 scavenging due to precipitation change caused by fire aerosols themselves. Hence, the

422 processes included in our simulations are closer to reality, and the results could better

423 reflect the nature of fire aerosol-convection interaction in the Maritime Continent.

424 Averaged through the entire modeled fire periods, cloud water mass (Qc), cloud

425 droplet number concentration (Qnc), and rain drop number concentration (Qnr) in FFBB

426 differ substantially from those in FF, demonstrating the influence of fire aerosols. Figure

427 8 shows that adding fire aerosols in FFBB would increase Qc by 14% and Qnc by 226%

428 in r1, and Qc by 18% and Qnc by 349% in r2. Another pronounced change in response to

429 adding fire aerosols is a decrease in Qnr by 44% in r1 and 47% in r2. Although an

430 increase in snow mass (Qs) and graupel mass (Qg) and a decrease in rain water mass (Qr)

431 after adding fire aerosols, the uncertainty of these hydrometeor changes is large.

432 In Sect. 3.2, we have discussed the significant rainfall increase occurred in the weak

433 convective systems after adding fire aerosols due to aerosol invigoration effect. On one

434 hand, regardless the strength of convection, the mean 3-hourly rainfall during the fire

435 periods is 1.06 ± 0.85 mm in FF and 1.09 ± 0.86 mm in FFBB over the Sumatra region (r1),

436 and statistically it does not change significantly in responding to fire aerosols. The

437 rainfall difference in the Borneo region (r2) between FF and FFBB is also insignificant

438 (1.32 ± 1.20 mm 3hrs^{-1} in FF versus 1.35 ± 1.14 mm 3hrs^{-1} in FFBB). On the other hand,

19

439   we have found that the impacts of fire aerosols appear in several other rainfall patterns.

440   For instance, the daily maximum and minimum rainfalls display clear differences

441   between the FFBB and FF simulations, specifically in r2 rather than in r1 (Fig. 9). While

442   for r1, the impacts of fire aerosol are reflected in event-wise statistics, e.g., higher event-

443   wise maximum and minimum rainfall intensity in FFBB than in FF, identified in 30 out

444   of 54 convective events in total. These are mostly weak convective events in r1.

445   Interestingly, somewhat opposite to the rainfall statistics in r1, the intensity of event-wise

446   maximum and minimum rainfall in r2 is higher in FF than in FFBB. The daily rainfall

447   peak of 3-hr rainfall in r1 is mostly less than 3 mm; in comparison, one-third of

448   convective events in r2 have daily maximum 3-hr rainfall exceeding 3 mm (Fig. 9c),

449   suggesting that the convective systems in r2 tend to develop stronger than in r1 and the

450   fire aerosols significantly suppress the maximum rainfall intensity of strong convections

451   in r1. We roughly used 1.25 mm $3hr^{-1}$ of the domain-averaged rainfall to classify weak

452   and strong convective systems. We find that the conclusions regarding differences of

453   hydrometers and rainfall in the weak systems between the FF and FFBB experiments stay

454   the same, and such differences are still not that significant in both regions (Table S1 and

455   Fig. S8).

456   We have categorized the maximum rainfall based on its values in the afternoon and

457   midnight. We find that those heavy maximum rainfalls in r2 tend to occur in the

458   midnight (Fig. 9c) associated with the anticyclonic circulation formed in the western

459   Borneo induced by southeasterly winds from the Southern latitude turn northeastward

460   along the west coast of Borneo, owing to the terrain of Borneo Island and the sea breezes

461   from the South China Sea. The vortex produced by such a circulation leads to strong

20

462   updraft and then strong convection.   Note that this anticyclonic circulation is different

463   from the Borneo vortex, the latter appears as a persistent feature of the boreal winter

464   climatology and is related to the northeasterly from the South China Sea and cold surge

465   events (Chang et al., 1983; Chang et al., 2005).

466   The low-level wind pattern of Borneo convections is similar to the westerly regime,

467   especially the weak westerly (WW) regime identified by Ichikawa and Yasunari (2006).

468   According to their analysis, the WW regime tends to occur in boreal summer. Its

469   composites include an anticyclonic feature with the weak wind field over the Borneo

470   Island. The deep convective storms developed in the WW regime tend to stay close to

471   the west coast associated with the lower-level convergence enhanced by the prevailing

472   wind and local circulations around there, resulting in localized rainfall over the offshore

473   region of the west coast. Based on our simulations, the onset of convection occurs in the

474   afternoon over the western mountain range of Borneo. These storms would consequently

475   evolve into widespread shallow storms in the evening over the western part of the island.

476   The maximum rainfall appears on the west coast because of a local westward propagating

477   rainfall system that develops around midnight or early morning.

478   The comparison of the maximum rainfall between FF and FFBB in Fig. 9 shows that

479   fire aerosols tend to reduce the maximum rainfall, especially for high-intensity rainfall

480   events.   In other words, fire aerosols have substantial impacts on the nocturnal

481   convections, which are associated with the local anticyclonic circulation in the western

482   Borneo. This effect on nocturnal convections in the western Borneo by fire aerosols will

483   be discussed further in the next section.

21

3.4 The impact of biomass burning aerosols on nocturnal convections in the Borneo region

To further analyze the effects of fire aerosols on nocturnal convections, we have categorized convective events into nocturnal convections (NC) and non-nocturnal convections (non-NC), based on whether the maximum rainfall occurs from midnight to early morning or in the time frame from late afternoon to evening. Figure 10 shows the diurnal time series of precipitation averaged over the Borneo region (r2) in FF and FFBB. Again, 3-hour-mean rainfalls of nocturnal convections are higher than those of non-nocturnal convections in both simulations and fire aerosols weaken the maximum nocturnal rainfall intensity about 9%.

Nocturnal convections tend to stay close to the west coast associated with a lower-level convergence enhanced by the prevailing wind and local circulations mainly related to the land breezes from inland of the western Borneo. The strong convergence near the surface over the offshore region of the west coast causes the weak westerly monsoon windflaws and local land breezes to merge during the nighttime. However, during the fire periods, the daytime absorption of fire aerosols (e.g., black carbon) can cause an atmospheric warming (even without fire generated heating flux being incorporated in the model). This could increase near surface air temperature, weaken land breezes and thus surface convergence. As a result, the nocturnal convections in FFBB cannot develop as strong as those in FF. On the other hand, both nocturnal and non-nocturnal convections are initiated over the western mountain range under a prevailing wind of the sea breezes from the South China Sea. The increases of near surface temperature owing to the fire

22

aerosols can enhance this prevailing wind from the ocean and thus lead to a higher
convective rainfall in FFBB during the onset stage of the nocturnal convections as well as
non-nocturnal convections. Figure 11 illustrates the sea breeze increase in FFBB during
the daytime (20 LST) and the land breeze decrease in FFBB during the nighttime (2
LST). Twenty LST and 2 LST are chosen here because of the peak of difference.

Diurnal evolution of vertical profiles clearly indicates that mass mixing ratio of total
hydrometeors, temperature, and vertical velocity differ in both daytime and nighttime
between FF and FFBB for those nocturnal convections (Fig. 12). The differences of near
surface temperature between FF and FFBB are more pronounced during the period after
sunset (Fig. 12d). The differences of near surface temperature mainly happen over land,
and the higher near surface temperature in FFBB weakens the land breezes and near
surface convergence along the coast. Starting from late afternoon, (about 5 PM local
time), vertical velocity increases with time until sunrise next day in both simulations (Fig.
12e) due to the convergence of the monsoon windflaws and local land breezes during the
nighttime, and this matches very well with that of mass mixing ratio of total
hydrometeors (Fig. 12a and 12e). Noticeably, the main differences in vertical velocity
and hydrometeor mass mixing ratio between FFBB and FF also start to become evident
after entering the evening. Because of the weaker convergence near the surface in FFBB,
the differences in vertical velocity at the higher altitude between FFBB and FF peaks in
the nighttime. The temperature increase from aerosol absorption seems small (please
note that the direct heating from fire is not included in the WRF fire plume model) but we
do see the change of vertical velocity owing to the aerosol heating effect. Based on our
analysis, the temperature increase is mainly associated with the thermodynamic

532 perturbation from the absorption of sunlight by fire aerosols. This seems also consistent

533 with the analysis of Zhang et al. (2019). Indeed, should the heat flux generated by fires

534 be incorporated in the model, the warming effects from biomass burning would be much

535 stronger and also persist in nocturnal timeframe.

536   As a summary, the schematics shown in Fig. 13 illustrate the impact of biomass

537 burning activities on nocturnal convections in the Borneo region. In the daytime, under

538 the prevailing wind of sea breezes from the South China Sea, convections develop over

539 the western mountain range. Because near surface heating from the absorption of

540 sunlight by fire aerosols could enhance the prevailing wind from the ocean, convective

541 rainfall becomes higher at the onset stage of the nocturnal convections (still in daytime)

542 due to biomass burning activities (Fig. 13b). In the nighttime, convection moves to the

543 offshore region of the western Borneo. The strong convergences near the surface merge

544 the weak westerly monsoon windflaws with local nighttime land breezes to form an

545 anticyclonic circulation (Fig. 13c). During the fire periods, the daytime near surface

546 warming by fire aerosols could also further weaken land breezes and surface

547 convergence. Hence, the nocturnal convections during fire events would not develop as

548 strong as in days without fires (Fig. 13d versus 13c).

549 **4 Summary**

550   By comparing WRF-Chem modeling results include or exclude biomass burning

551 emissions (FFBB versus FF), we have identified certain detailed impacts of fire aerosols

552 on convective events within two study regions in the Maritime Continent during a four-

553 month period (June 2008 ~ September 2008). In total, 54 convective systems in the

554 Sumatra region and 35 convective systems in the Borneo region have been simulated.

555 Three convective events of each study region have been selected for in-depth

556 investigation. In addition, statistical analyses have been performed throughout the entire

557 simulation period for each region. We have focused our analyses on two rainfall

558 features: 1) convective precipitation associated with Sumatra squall lines, and 2) diurnal

559 rainfall over the western Borneo.

560 We find that fire aerosols lead to the increase of cloud water mass and cloud droplet

561 number concentration among all analyzed cases while a substantial reduction of rain drop

562 number concentration. Influences of fire aerosols on other hydrometeors vary from case

563 to case. Specifically, our results show that fire aerosols can significantly change the

564 quantities of hydrometeors, particularly those involved in cold cloud processes and

565 rainfall of weak convections in either the Sumatra region or the Borneo region. Rainfall

566 intensity is higher in FFBB during the entire convection life cycle in those weak

567 convection cases, and the nighttime rainfall intensity in FFBB is significantly higher than

568 that in FF.

569 Statistics performed throughout the entire modeled fire season shows that the fire

570 aerosols only cause a nearly negligible change (2-3%) to the total rainfall of convective

571 systems in both study regions. On the other hand, we notice that fire aerosols can still

572 alter daily maximum and minimum rainfall in some cases, for example, fire aerosols lead

573 to the increase of maximum and minimum rainfall intensity in 30 weak convective events

574 in the Sumatra region.

575 In the Borneo region, biomass burning activities mainly affect the rainfall intensity

576 of nocturnal convection. Because near surface heating from the absorption of fire

25

577 aerosols can enhance the prevailing wind from the ocean (sea breeze) during the daytime,

578 the convective rainfall over the western mountain range is higher during the onset stage

579 of the nocturnal convections. In the nighttime, the consequence of the above

580 thermodynamic perturbation by absorbing fire aerosols can further weaken land breeze

581 and surface convergence. Hence, the rainfall intensity of nocturnal convections under the

582 influence of fire aerosols would become weaker by about 9%.

583   This study has demonstrated how biomass burning activities could affect convective

584 systems in the Maritime Continent by altering cloud microphysics and dynamics. We

585 find the biomass burning activities significantly change the diurnal rainfall intensity,

586 especially those low-level wind patterns associated with the weak westerly (WW) regime

587 as suggested by Ichikawa and Yasunari (2006). Our results show that neither a single

588 case study nor a simple statistical summary applied to overall model simulation period

589 without in-depth analyses could reveal the impact of biomass burning aerosols on

590 convections under different windflaw regimes.

591 **Data availability**

592   FINNv1.5 emission data are publicly available from

593 http://bai.acom.uar.edu/Data/fire/. REAS emission data can be downloaded from

594 https://www.nies.go.jp/REAS/. TRMM data can be obtained from

595 https://pmm.nasa.gov/data-access/downloads/trmm. AOD from MODIS can be

596 obtained from http://dx.doi.org/10.5067/MODIS/MOD08_M3.061. Sounding profiles

597 are publicly available on http://weather.uwyo.edu/upperair/sounding.html. WRF-Chem

598 simulated data are available upon request from Hsiang-He Lee (lee1061@llnl.gov).

26

Author contribution

H.-H. L. and C. W. designed the experiments and H.-H. L. carried them out. H.-H. L. configured the simulations and analyzed the results. H.-H. L. and C. W. wrote the manuscript.

Acknowledgments

27

Reference:

Ackermann, I. J., Hass, H., Memmesheimer, M., Ebel, A., Binkowski, F. S., and Shankar, U.: Modal aerosol dynamics model for Europe: development and first applications, Atmospheric Environment, 32, 2981-2999, http://dx.doi.org/10.1016/S1352-2310(98)00006-5, 1998.

Andreae, M. O., and Gelencsér, A.: Black carbon or brown carbon? The nature of light-absorbing carbonaceous aerosols, Atmos. Chem. Phys., 6, 3131-3148, 10.5194/acp-6-3131-2006, 2006.

Chang, C.-P., Millard, J. E., and Chen, G. T. J.: Gravitational Character of Cold Surges during Winter MONEX, Monthly Weather Review, 111, 293-307, 10.1175/1520-0493(1983)111<0293:gcocsd>2.0.co;2, 1983.

Chang, C.-P., Harr, P. A., and Chen, H.-J.: Synoptic Disturbances over the Equatorial South China Sea and Western Maritime Continent during Boreal Winter, Monthly Weather Review, 133, 489-503, 10.1175/mwr-2868.1, 2005.

Crippa, P., Castruccio, S., Archer-Nicholls, S., Lebron, G. B., Kuwata, M., Thota, A., Sumin, S., Butt, E., Wiedinmyer, C., and Spracklen, D. V.: Population exposure to hazardous air quality due to the 2015 fires in Equatorial Asia, Scientific Reports, 6, 37074, 10.1038/srep37074, 2016.

Fan, J., Rosenfeld, D., Zhang, Y., Giangrande, S. E., Li, Z., Machado, L. A. T., Martin, S. T., Yang, Y., Wang, J., Artaxo, P., Barbosa, H. M. J., Braga, R. C., Comstock, J. M., Feng, Z., Gao, W., Gomes, H. B., Mei, F., Pöhlker, C., Pöhlker, M. L., Pöschl, U., and de Souza, R. A. F.: Substantial convection and precipitation enhancements by ultrafine aerosol particles, Science, 359, 411-418, 10.1126/science.aan8461, 2018.

Frankenberg, E., McKee, D., and Thomas, D.: Health consequences of forest fires in Indonesia, Demography, 42, 109-129, 10.1353/dem.2005.0004, 2005.

Freitas, S. R., Longo, K. M., Chatfield, R., Latham, D., Silva Dias, M. A. F., Andreae, M. O., Prins, E., Santos, J. C., Gielow, R., and Carvalho Jr, J. A.: Including the sub-grid scale plume rise of vegetation fires in low resolution atmospheric transport models, Atmos. Chem. Phys., 7, 3385-3398, 10.5194/acp-7-3385-2007, 2007.

Fujii, Y., Iriana, W., Oda, M., Puriwigati, A., Tohno, S., Lestari, P., Mizohata, A., and Huboyo, H. S.: Characteristics of carbonaceous aerosols emitted from peatland fire in Riau, Sumatra, Indonesia, Atmospheric Environment, 87, 164-169, http://dx.doi.org/10.1016/j.atmosenv.2014.01.037, 2014.

Ge, C., Wang, J., and Reid, J. S.: Mesoscale modeling of smoke transport over the Southeast Asian Maritime Continent: coupling of smoke direct radiative effect below and above the low-level clouds, Atmos. Chem. Phys., 14, 159-174, 10.5194/acp-14-159-2014, 2014.

Grandey, B. S., Lee, H. H., and Wang, C.: Radiative effects of interannually varying vs. interannually invariant aerosol emissions from fires, Atmos. Chem. Phys., 16, 14495-14513, 10.5194/acp-16-14495-2016, 2016.

Grell, G. A., Peckham, S. E., Schmitz, R., McKeen, S. A., Frost, G., Skamarock, W. C., and Eder, B.: Fully coupled "online" chemistry within the WRF model, Atmospheric Environment, 39, 6957-6975, 10.1016/j.atmosenv.2005.04.027, 2005.

662   Grell, G. A., and Freitas, S. R.: A scale and aerosol aware stochastic convective
663 parameterization for weather and air quality modeling, Atmos. Chem. Phys., 14,
664 5233-5250, 10.5194/acp-14-5233-2014, 2014.
665   Hodzic, A., and Duvel, J. P.: Impact of Biomass Burning Aerosols on the Diurnal
666 Cycle of Convective Clouds and Precipitation Over a Tropical Island, Journal of
667 Geophysical Research: Atmospheres, 123, 1017-1036, 10.1002/2017JD027521,
668 2017.
669   Huffman, G. J., Bolvin, D. T., Nelkin, E. J., Wolff, D. B., Adler, R. F., Gu, G., Hong, Y.,
670 Bowman, K. P., and Stocker, E. F.: The TRMM Multisatellite Precipitation Analysis
671 (TMPA): Quasi-Global, Multiyear, Combined-Sensor Precipitation Estimates at Fine
672 Scales, Journal of Hydrometeorology, 8, 38-55, 10.1175/JHM560.1, 2007.
673   Iacono, M. J., Delamere, J. S., Mlawer, E. J., Shephard, M. W., Clough, S. A., and
674 Collins, W. D.: Radiative forcing by long-lived greenhouse gases: Calculations with
675 the AER radiative transfer models, Journal of Geophysical Research: Atmospheres,
676 113, 10.1029/2008JD009944, 2008.
677   Ichikawa, H., and Yasunari, T.: Time–Space Characteristics of Diurnal Rainfall
678 over Borneo and Surrounding Oceans as Observed by TRMM-PR, Journal of Climate,
679 19, 1238-1260, 10.1175/jcli3714.1, 2006.
680   Jeong, G. R., and Wang, C.: Climate effects of seasonally varying Biomass Burning
681 emitted Carbonaceous Aerosols (BBCA), Atmos. Chem. Phys., 10, 8373-8389,
682 10.5194/acp-10-8373-2010, 2010.
683   Jiang, J. H., Su, H., Huang, L., Wang, Y., Massie, S., Zhao, B., Omar, A., and Wang, Z.:
684 Contrasting effects on deep convective clouds by different types of aerosols, Nature
685 Communications, 9, 3874, 10.1038/s41467-018-06280-4, 2018.
686   Koh, T.-Y., and Teo, C.-K.: TOWARD A MESOSCALE OBSERVATION NETWORK IN
687 SOUTHEAST ASIA, Bulletin of the American Meteorological Society, 90, 481-488,
688 10.1175/2008bams2561.1, 2009.
689   Kunii, O., Kanagawa, S., Yajima, I., Hisamatsu, Y., Yamamura, S., Amagai, T., and
690 Ismail, I. T. S.: The 1997 Haze Disaster in Indonesia: Its Air Quality and Health
691 Effects, Archives of Environmental Health: An International Journal, 57, 16-22,
692 10.1080/00039890209602912, 2002.
693   Kurokawa, J., Ohara, T., Morikawa, T., Hanayama, S., Janssens-Maenhout, G.,
694 Fukui, T., Kawashima, K., and Akimoto, H.: Emissions of air pollutants and
695 greenhouse gases over Asian regions during 2000–2008: Regional Emission
696 inventory in ASia (REAS) version 2, Atmos. Chem. Phys., 13, 11019-11058,
697 10.5194/acp-13-11019-2013, 2013.
698   Lee, H.-H., Bar-Or, R. Z., and Wang, C.: Biomass burning aerosols and the low-
699 visibility events in Southeast Asia, Atmos. Chem. Phys., 17, 965-980, 10.5194/acp-
700 17-965-2017, 2017.
701   Lee, H.-H., Iraqui, O., Gu, Y., Yim, S. H. L., Chulakadabba, A., Tonks, A. Y. M., Yang,
702 Z., and Wang, C.: Impacts of air pollutants from fire and non-fire emissions on the
703 regional air quality in Southeast Asia, Atmos. Chem. Phys., 18, 6141-6156,
704 10.5194/acp-18-6141-2018, 2018.
705   Lee, H.-H., Iraqui, O., and Wang, C.: The Impact of Future Fuel Consumption on
706 Regional Air Quality in Southeast Asia, Scientific Reports, 9, 2648, 10.1038/s41598-
707 019-39131-3, 2019.

708   Lin, J. C., Matsui, T., Pielke Sr., R. A., and Kummerow, C.: Effects of biomass-
709 burning-derived aerosols on precipitation and clouds in the Amazon Basin: a
710 satellite-based empirical study, Journal of Geophysical Research: Atmospheres, 111,
711 10.1029/2005jd006884, 2006.
712   Lin, N.-H., Tsay, S.-C., Maring, H. B., Yen, M.-C., Sheu, G.-R., Wang, S.-H., Chi, K. H.,
713 Chuang, M.-T., Ou-Yang, C.-F., Fu, J. S., Reid, J. S., Lee, C.-T., Wang, L.-C., Wang, J.-L.,
714 Hsu, C. N., Sayer, A. M., Holben, B. N., Chu, Y.-C., Nguyen, X. A., Sopajaree, K., Chen, S.-
715 J., Cheng, M.-T., Tsuang, B.-J., Tsai, C.-J., Peng, C.-M., Schnell, R. C., Conway, T., Chang,
716 C.-T., Lin, K.-S., Tsai, Y. I., Lee, W.-J., Chang, S.-C., Liu, J.-J., Chiang, W.-L., Huang, S.-J.,
717 Lin, T.-H., and Liu, G.-R.: An overview of regional experiments on biomass burning
718 aerosols and related pollutants in Southeast Asia: From BASE-ASIA and the Dongsha
719 Experiment to 7-SEAS, Atmospheric Environment, 78, 1-19,
720 http://dx.doi.org/10.1016/j.atmosenv.2013.04.066, 2013.
721   Lo, J. C. F., and Orton, T.: The general features of tropical Sumatra Squalls,
722 Weather, 71, 175-178, 10.1002/wea.2748, 2016.
723   Miettinen, J., Shi, C., and Liew, S. C.: Deforestation rates in insular Southeast Asia
724 between 2000 and 2010, Global Change Biology, 17, 2261-2270, 10.1111/j.1365-
725 2486.2011.02398.x, 2011.
726   Mlawer, E. J., Taubman, S. J., Brown, P. D., Iacono, M. J., and Clough, S. A.:
727 Radiative transfer for inhomogeneous atmospheres: RRTM, a validated correlated-k
728 model for the longwave, Journal of Geophysical Research: Atmospheres, 102, 16663-
729 16682, 10.1029/97JD00237, 1997.
730   Morrison, H., Curry, J. A., and Khvorostyanov, V. I.: A New Double-Moment
731 Microphysics Parameterization for Application in Cloud and Climate Models. Part I:
732 Description, Journal of the Atmospheric Sciences, 62, 1665-1677,
733 10.1175/jas3446.1, 2005.
734   Morrison, H., Thompson, G., and Tatarskii, V.: Impact of Cloud Microphysics on
735 the Development of Trailing Stratiform Precipitation in a Simulated Squall Line:
736 Comparison of One- and Two-Moment Schemes, Monthly Weather Review, 137,
737 991-1007, 10.1175/2008mwr2556.1, 2009.
738   Nakanishi, M., and Niino, H.: Development of an Improved Turbulence Closure
739 Model for the Atmospheric Boundary Layer, Journal of the Meteorological Society of
740 Japan. Ser. II, 87, 895-912, 10.2151/jmsj.87.895, 2009.
741   National Centers for Environmental Prediction, N. W. S. N. U. S. D. o. C.: NCEP FNL
742 Operational Model Global Tropospheric Analyses, continuing from July 1999,
743 10.5065/D6M043C6, 2000.
744   Oki, T., and Musiake, K.: Seasonal Change of the Diurnal Cycle of Precipitation
745 over Japan and Malaysia, Journal of Applied Meteorology, 33, 1445-1463,
746 10.1175/1520-0450(1994)033<1445:scotdc>2.0.co;2, 1994.
747   Ramanathan, V., Crutzen, P. J., Lelieveld, J., Mitra, A. P., Althausen, D., Anderson, J.,
748 Andreae, M. O., Cantrell, W., Cass, G. R., Chung, C. E., Clarke, A. D., Coakley, J. A.,
749 Collins, W. D., Conant, W. C., Dulac, F., Heintzenberg, J., Heymsfield, A. J., Holben, B.,
750 Howell, S., Hudson, J., Jayaraman, A., Kiehl, J. T., Krishnamurti, T. N., Lubin, D.,
751 McFarquhar, G., Novakov, T., Ogren, J. A., Podgorny, I. A., Prather, K., Priestley, K.,
752 Prospero, J. M., Quinn, P. K., Rajeev, K., Rasch, P., Rupert, S., Sadourny, R., Satheesh, S.
753 K., Shaw, G. E., Sheridan, P., and Valero, F. P. J.: Indian Ocean Experiment: An

754 integrated analysis of the climate forcing and effects of the great Indo-Asian haze,
755 Journal of Geophysical Research: Atmospheres, 106, 28371-28398,
756 10.1029/2001jd900133, 2001.
757 Ramanathan, V., and Carmichael, G.: Global and regional climate changes due to
758 black carbon, Nature Geosci, 1, 221-227, 2008.
759 Rosenfeld, D.: TRMM observed first direct evidence of smoke from forest fires
760 inhibiting rainfall, Geophysical Research Letters, 26, 3105-3108,
761 10.1029/1999gl006066, 1999.
762 Rosenfeld, D., Lohmann, U., Raga, G. B., O'Dowd, C. D., Kulmala, M., Fuzzi, S.,
763 Reissell, A., and Andreae, M. O.: Flood or Drought: How Do Aerosols Affect
764 Precipitation?, Science, 321, 1309-1313, 10.1126/science.1160606, 2008.
765 Satheesh, S. K., and Ramanathan, V.: Large differences in tropical aerosol forcing
766 at the top of the atmosphere and Earth's surface, Nature, 405, 60-63,
767 10.1038/35011039, 2000.
768 Schell, B., Ackermann, I. J., Hass, H., Binkowski, F. S., and Ebel, A.: Modeling the
769 formation of secondary organic aerosol within a comprehensive air quality model
770 system, Journal of Geophysical Research: Atmospheres (1984–2012), 106, 28275-
771 28293, 2001.
772 Sekiguchi, M., Nakajima, T., Suzuki, K., Kawamoto, K., Higurashi, A., Rosenfeld, D.,
773 Sano, I., and Mukai, S.: A study of the direct and indirect effects of aerosols using
774 global satellite data sets of aerosol and cloud parameters, Journal of Geophysical
775 Research: Atmospheres, 108, 4699, 10.1029/2002JD003359, 2003.
776 Shi, H., Jiang, Z., Zhao, B., Li, Z., Chen, Y., Gu, Y., Jiang, J. H., Lee, M., Liou, K.-N., Neu,
777 J. L., Payne, V. H., Su, H., Wang, Y., Witek, M., and Worden, J.: Modeling Study of the
778 Air Quality Impact of Record-Breaking Southern California Wildfires in December
779 2017, Journal of Geophysical Research: Atmospheres, 124, 6554-6570,
780 10.1029/2019jd030472, 2019.
781 Stockwell, W. R., Kirchner, F., Kuhn, M., and Seefeld, S.: A new mechanism for
782 regional atmospheric chemistry modeling, Journal of Geophysical Research:
783 Atmospheres, 102, 25847-25879, 10.1029/97JD00849, 1997.
784 Taylor, D.: Biomass burning, humans and climate change in Southeast Asia,
785 Biodivers Conserv, 19, 1025-1042, 10.1007/s10531-009-9756-6, 2010.
786 Tewari, M., F. Chen, W. Wang, J. Dudhia, M. A. LeMone, K. Mitchell, M. Ek, G.
787 Gayno, J. Wegiel, and Cuenca, R. H.: Implementation and verification of the unified
788 NOAH land surface model in the WRF model, 20th conference on weather analysis
789 and forecasting/16th conference on numerical weather prediction, Seattle, WA,
790 U.S.A., 2004.
791 Tosca, M. G., Randerson, J. T., and Zender, C. S.: Global impact of smoke aerosols
792 from landscape fires on climate and the Hadley circulation, Atmos. Chem. Phys., 13,
793 5227-5241, 10.5194/acp-13-5227-2013, 2013.
794 Wagner, A., Heinzeller, D., Wagner, S., Rummler, T., and Kunstmann, H.: Explicit
795 Convection and Scale-Aware Cumulus Parameterizations: High-Resolution
796 Simulations over Areas of Different Topography in Germany, Monthly Weather
797 Review, 146, 1925-1944, 10.1175/mwr-d-17-0238.1, 2018.

798 Wang, C.: A modeling study on the climate impacts of black carbon aerosols,
799 Journal of Geophysical Research: Atmospheres, 109, n/a-n/a,
800 10.1029/2003JD004084, 2004.
801 Wang, C.: A modeling study of the response of tropical deep convection to the
802 increase of cloud condensation nuclei concentration: 1. Dynamics and microphysics,
803 Journal of Geophysical Research: Atmospheres, 110, D21211,
804 10.1029/2004JD005720, 2005.
805 Wiedinmyer, C., Akagi, S. K., Yokelson, R. J., Emmons, L. K., Al-Saadi, J. A., Orlando,
806 J. J., and Soja, A. J.: The Fire INventory from NCAR (FINN): a high resolution global
807 model to estimate the emissions from open burning, Geosci. Model Dev., 4, 625-641,
808 10.5194/gmd-4-625-2011, 2011.
809 Wu, P., Hara, M., Hamada, J.-i., Yamanaka, M. D., and Kimura, F.: Why a Large
810 Amount of Rain Falls over the Sea in the Vicinity of Western Sumatra Island during
811 Nighttime, Journal of Applied Meteorology and Climatology, 48, 1345-1361,
812 10.1175/2009jamc2052.1, 2009.
813 Wu, R., Wen, Z., and He, Z.: ENSO Contribution to Aerosol Variations over the
814 Maritime Continent and the Western North Pacific during 2000–10, Journal of
815 Climate, 26, 6541-6560, 10.1175/JCLI-D-12-00253.1, 2013.
816 Yi, L., and Lim, H.: Semi-Idealized COAMPS®* Simulations of Sumatra Squall
817 Lines: the Role of Boundary Forcing, in: Advances in Geosciences, 111-124, 2006.
818 Zhang, Y., Fan, J., Logan, T., Li, Z., and Homeyer, C. R.: Wildfire impact on
819 environmental thermodynamics and severe convective storms, Geophysical
820 Research Letters, 0, 10.1029/2019gl084534, 2019.
821 Zhao, B., Gu, Y., Liou, K.-N., Wang, Y., Liu, X., Huang, L., Jiang, J. H., and Su, H.:
822 Type-Dependent Responses of Ice Cloud Properties to Aerosols From Satellite
823 Retrievals, Geophysical Research Letters, 45, 3297-3306, 10.1002/2018gl077261,
824 2018.
825

826

827   Table 1. The case period of the selected cases in the Sumatra region (r1) and the Borneo
828   region (r2)

Case name	Case period
r1c1	2008/08/10 0900 UTC ~ 2008/08/11 0300 UTC
r1c2	2008/08/19 0600 UTC ~ 2008/08/20 0000 UTC
r1c3	2008/09/23 0900 UTC ~ 2008/09/24 0000 UTC
r2c1	2008/08/05 0900 UTC ~ 2008/08/06 0300 UTC
r2c2	2008/09/17 0600 UTC ~ 2008/09/17 2100 UTC
r2c3	2008/09/22 0300 UTC ~ 2008/09/23 0000 UTC

829
830
831

33

832

Table 2. The fire periods in the two study regions

The Sumatra region (r1)	The Borneo region (r2)
6/10/2008 ~ 6/20/2008	6/21/2008 ~ 6/27/2008
6/25/2008 ~ 6/28/2008	8/1/2008 ~ 8/8/2008
7/4/2008 ~ 7/7/2008	9/10/2008 ~ 9/30/2008
7/27/2008 ~ 8/20/2008	
9/17/2008 ~ 9/27/2008	

833
834

835 Table 3. The mean differences in percentage of FFBB to FF (i.e. (FFBB-FF)/FF × 100%)
836 for each selected case over the main convection area in the Sumatra region (r1) and the
837 Borneo region (r2). Qc, Qi, Qr, Qs and Qg represents cloud, ice, rain, snow, and graupel
838 mass concentration respectively. Qnc, Qni, Qnr, Qns and Qng means number
839 concentration for each hydrometeor.

Case	Qc	Qi	Qr	Qs	Qg	Qnc	Qni	Qnr	Qns	Qng
r1c1	8%	27%	49%	62%	48%	248%	55%	-41%	33%	39%
r1c2	20%	-6%	-15%	-25%	1%	349%	-1%	-45%	-11%	-6%
r1c3	18%	10%	-10%	3%	5%	311%	4%	-50%	11%	-6%
r2c1	27%	1%	-6%	-5%	-4%	703%	3%	-59%	4%	-5%
r2c2	22%	10%	64%	69%	58%	337%	24%	-32%	17%	57%
r3c3	8%	10%	19%	60%	-2%	409%	-5%	-66%	8%	-12%

840

35

841 Table 4. The averaged precipitation (mm 3hrs^{-1}) of FFBB and FF for each selected case
842 over the main convection area in the Sumatra region (r1) and the Borneo region (r2).
843 Parentheses in the third column show the difference in percentage of FFBB to FF (i.e.
844 (FFBB-FF)/FF × 100%).
845

Case	FF	FFBB
r1c1	1.33±0.47	2.74±1.21 (+106%)
r1c2	2.97±1.42	3.05±1.49 (+3%)
r1c3	4.32±1.84	3.98±2.18 (-8%)
r2c1	3.73±2.64	3.07±1.21 (-18%)
r2c2	1.88±0.53	3.97±1.47 (+111%)
r3c3	0.54±0.53	1.10±1.02 (+103%)

846
847

36
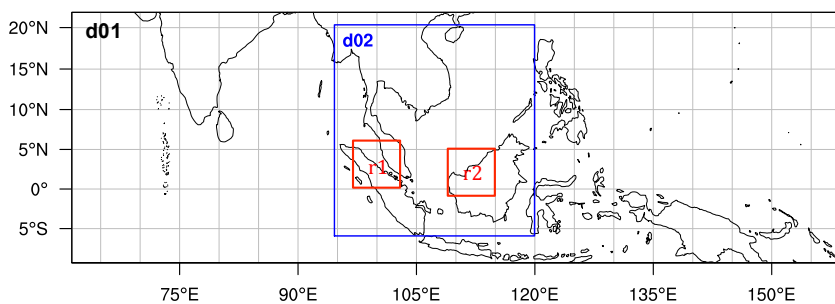
848
849   Figure 1. Domain configuration for WRF-Chem simulations. Domain 1 (d01) has a
850   resolution of 25 km, while Domain 2 (d02) has a resolution of 5 km. Two red boxes
851   indicate the two study regions: the Sumatra region (r1) and the Borneo region (r2).
852
853
854

(a) TRMM Precipitation (mm/day) - 2008

(b) FFBB Precipitation (mm/day) - 2008
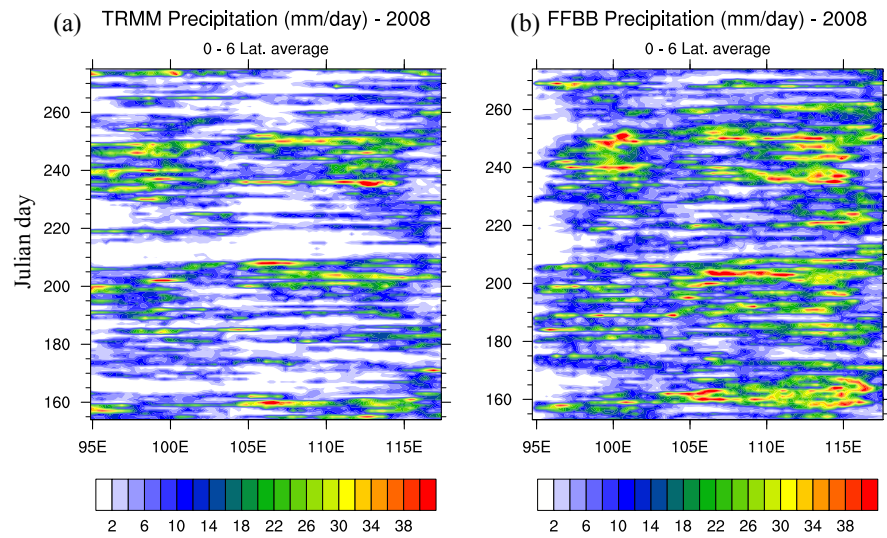
855
856 Figure 2. Hovmöller (time versus longitude) plot of daily precipitation (mm day^{-1}) from 1
857 June 2008 to 30 September 2008 from:(a) Tropical Rainfall Measuring Mission (TRMM)
858 and (b) FFBB. Latitude average is from 0° to 6°N.
859

38

(a) Rainfall comparison – r1

860

(b) Rainfall comparison – r2
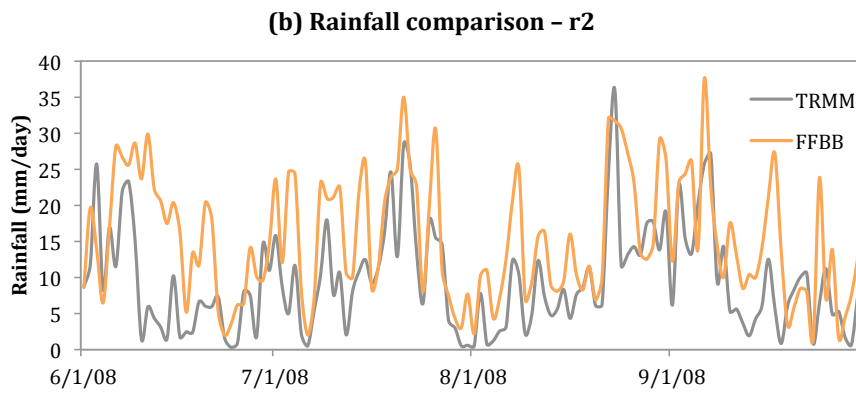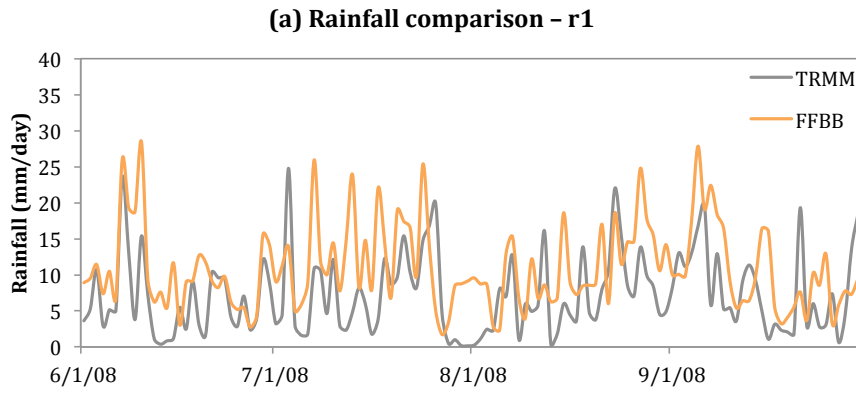
861
862 Figure 3. Time series of area-averaged daily rainfall (mm day^{-1}) from Tropical Rainfall
863 Measuring Mission (TRMM) and FFBB over (a) the Sumatra region (r1) and (b) the
864 Borneo region (r2).
865

39
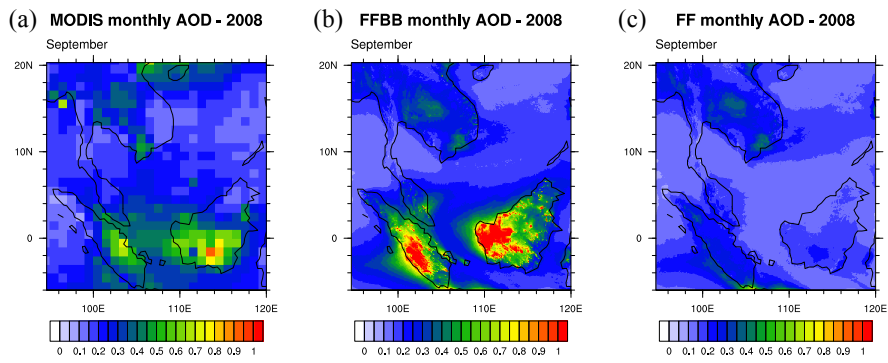
866
867 Figure 4. Monthly aerosol optical depth (AOD) in September 2008 from (a) Moderate
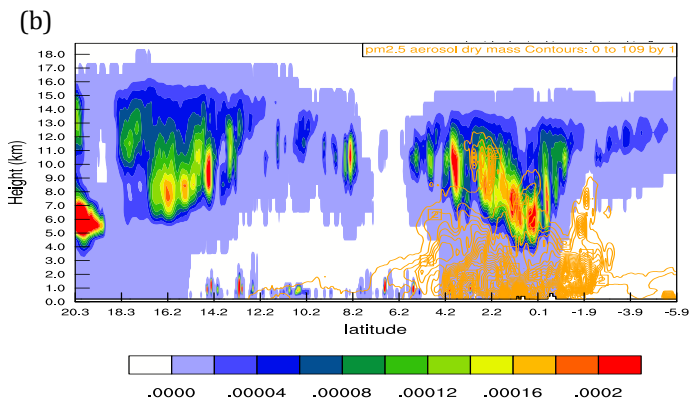868 Resolution Imaging Spectroradiometer (MODIS), (b) FFBB, and (c) FF.
869
870

(a)

(b)

871
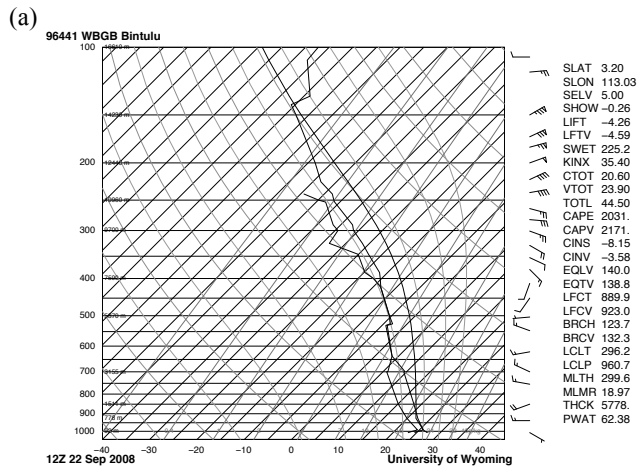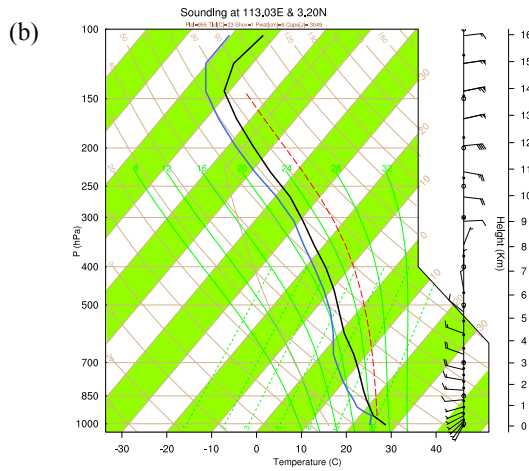
872
873 Figure 5. (a) Sounding profile observed at Bintulu Airport, Malaysia (113.03° E, 3.20° N)
874 at 12 UTC on 22 September 2008. (b) Modeled sounding profile in FFBB at the same
875 location and time as (a).

41

(a)

Vertical Feature Mask   UTC: 2008-09-22   18:16:05.2 to 2008-09-22   18:29:33.9   Version: 4.10 Standard Nighttime

7	(black)
6	(gray)
5	(green)
4	(yellow)
3	(orange)
3 (L)	(brown)
2	(cyan)
2 (L)	(magenta)
1	(blue)

Altitude, km

Lat	30.49	24.40	18.30	12.19	6.08	-0.03	-6.15	-12.26	-18.31
Lon	117.34	115.80	114.36	112.99	111.67	110.36	109.06	107.73	106.37

1 = clear air   2 = cloud   3 = tropospheric aerosol   4 = stratospheric aerosol   5 = surface   6 = subsurface   7= totally attenuated   L = low/no confidence

(b)

pm2.5 aerosol dry mass Contours: 0 to 109 by 1

Height (km)

latitude

.0000   .00004   .00008   .00012   .00016   .0002

(c)

pm2.5 aerosol dry mass Contours: 0 to 15 by 1

Height (km)

latitude

.0000   .00004   .00008   .00012   .00016   .0002

876
877
878

879

42

880   Figure 6 (a) The vertical structure of cloud retrieved from the Cloud-Aerosol Lidar and Infrared Pathfinder Satellite Observation
881   (CALIPSO) on September 22, 2008. (b)-(c) The sum of simulated hydrometeor mixing ratio (shaded; kg kg^{-1}) and PM$_{2.5}$ concentration
882   (contour; μg m^{-3}) in FFBB and FF, respectively. The profile domain of (b) and (c) is corresponding to the red rectangle in (a).
883

43
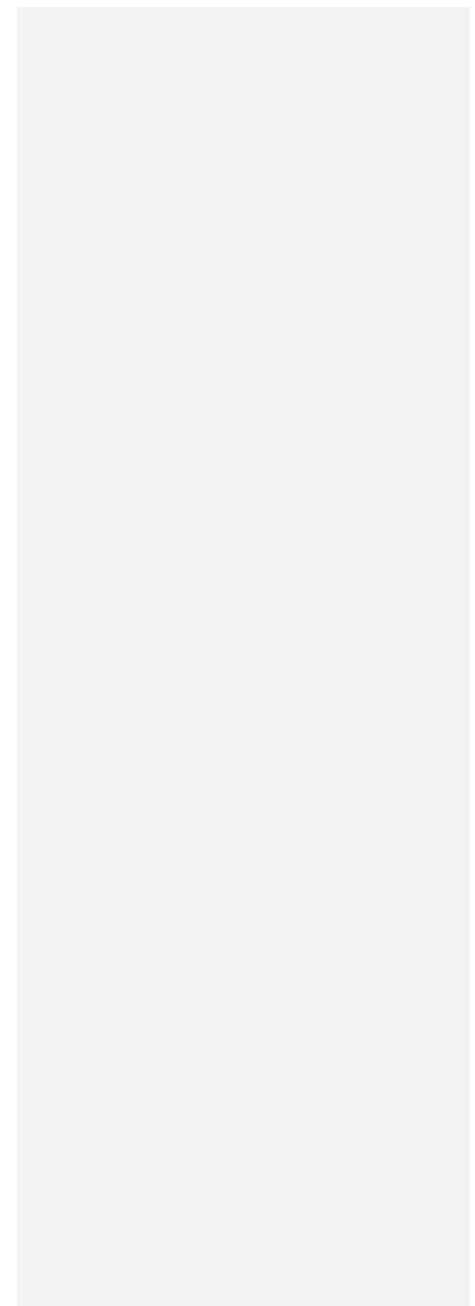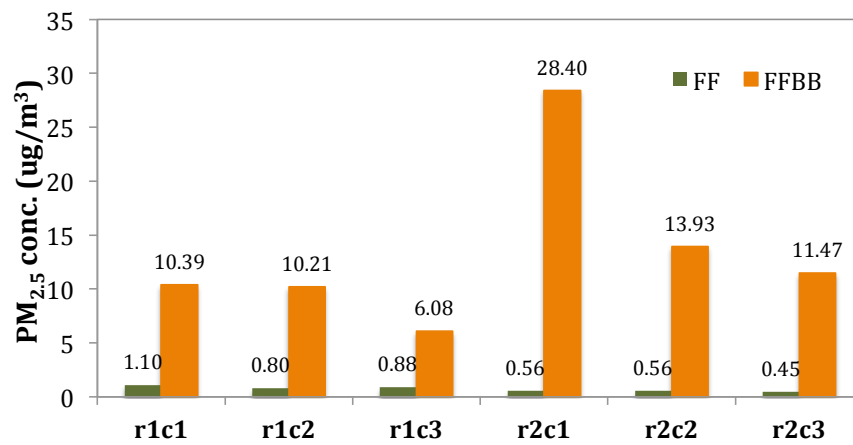
Figure 7. The mean PM$_{2.5}$ concentration (µg m^{-3}) in FF and FFBB for selected cases in the Sumatra region (r1) and the Borneo region (r2).

888
889
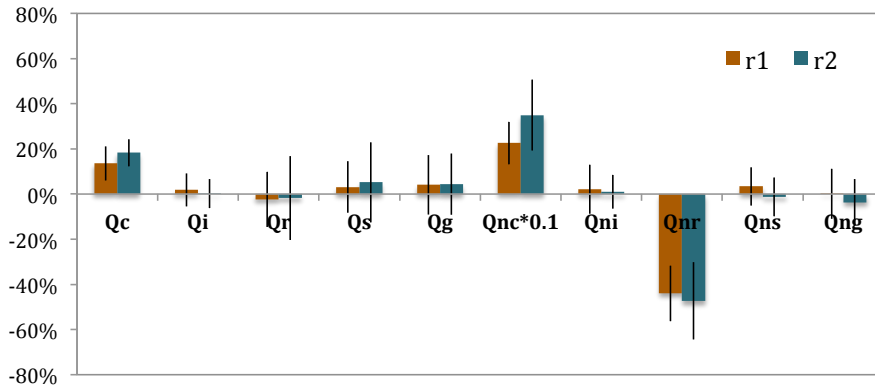
890
891 Figure 8. The mean differences in percentage of FFBB to FF (i.e. (FFBB-FF)/FF × 100%)
892 over all convective cases during the fire periods in the Sumatra region (r1) and the Borneo
893 region (r2). Qc, Qi, Qr, Qs and Qg represents cloud, ice, rain, snow, and graupel mass
894 concentration, respectively. Qnc, Qni, Qnr, Qns and Qng means number concentration for
895 each hydrometeor. The error bars represent one standard deviation.
896
897
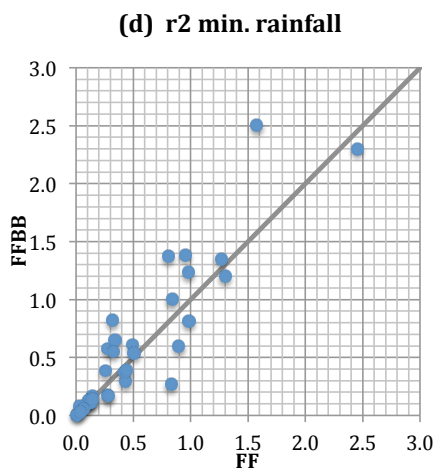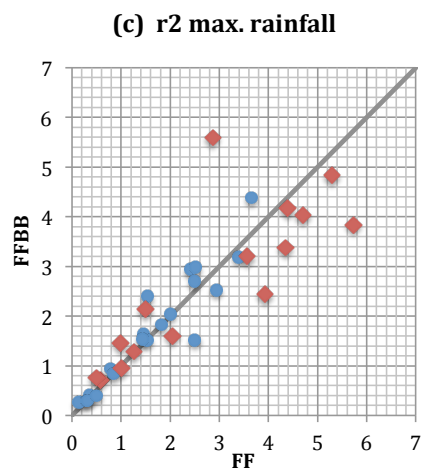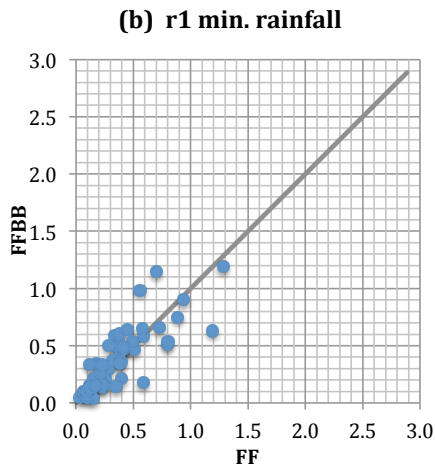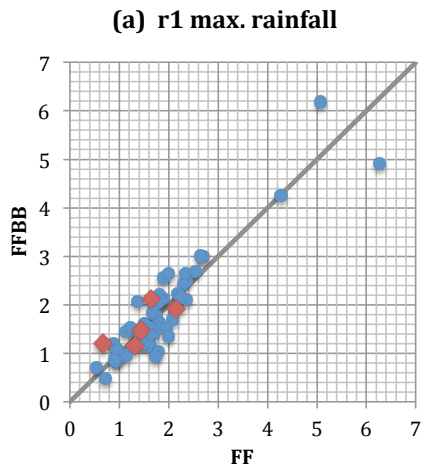
898

899

900   Figure 9. The scatterplots of daily maximum and minimum convective rainfall (mm $3hr^{-1}$)
901   during the fire periods in in the Sumatra region (r1) and the Borneo region (r2). Red
902   diamonds in (a) and (c) indicate that the maximum convective rainfall conducts in the
903   midnight or early morning.

904

905

46
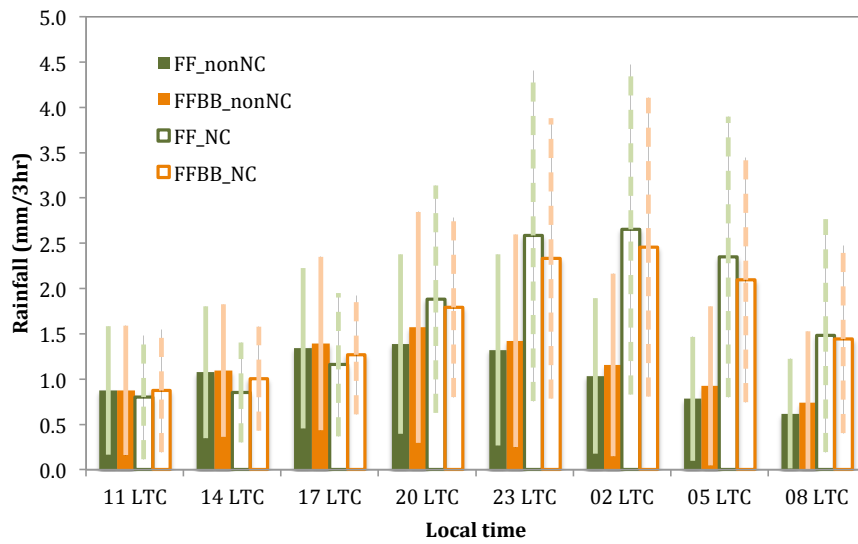
Figure 10. The diurnal time series of rainfall averaged over the Borneo region (r2) for nocturnal convections (NC) and non- nocturnal convections (non-NC) during fire periods in FF and FFBB. The error bars denote the standard deviation of the rainfall.

(a)

912
(b)
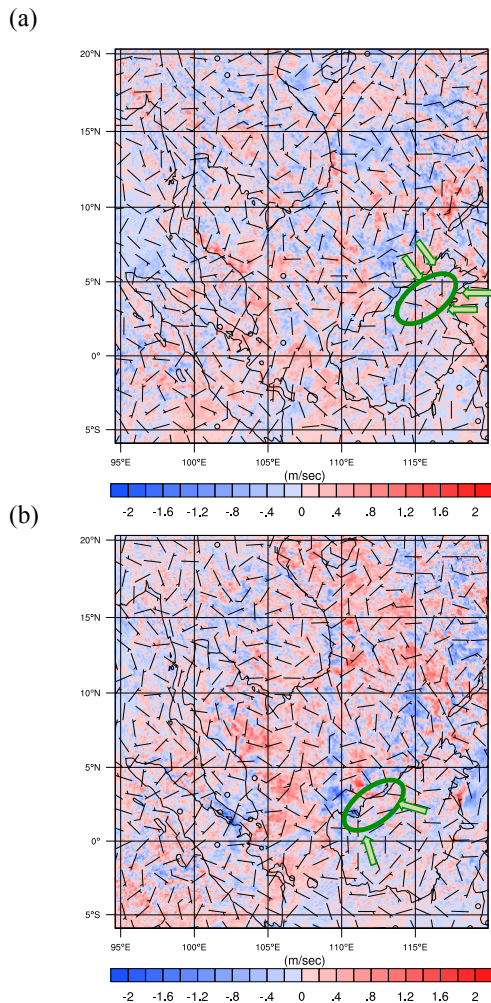
913
914 Figure 11. The mean wind field differences of FFBB and FF (FFBB-FF) at (a) 20 LST for
915 non-nocturnal cases and (b) 02 LST for nocturnal cases in the Borneo region (r2). The green
916 circle indicates the location of convections occurred. The green arrows mean the mean flow
917 of sea breeze in (a) and land breeze in (b). The magnitude of wind barbs is 10 times higher
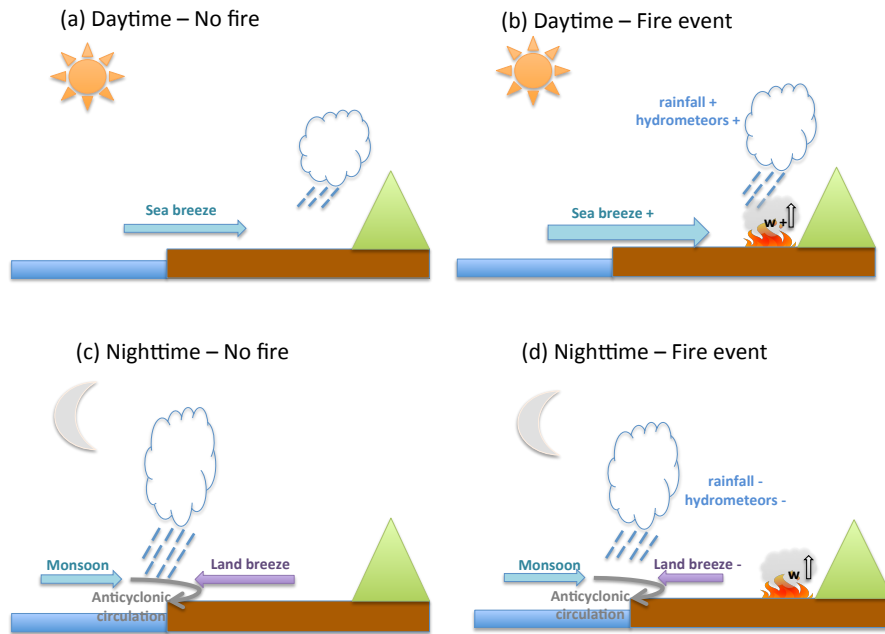918 than the real value.
919
920
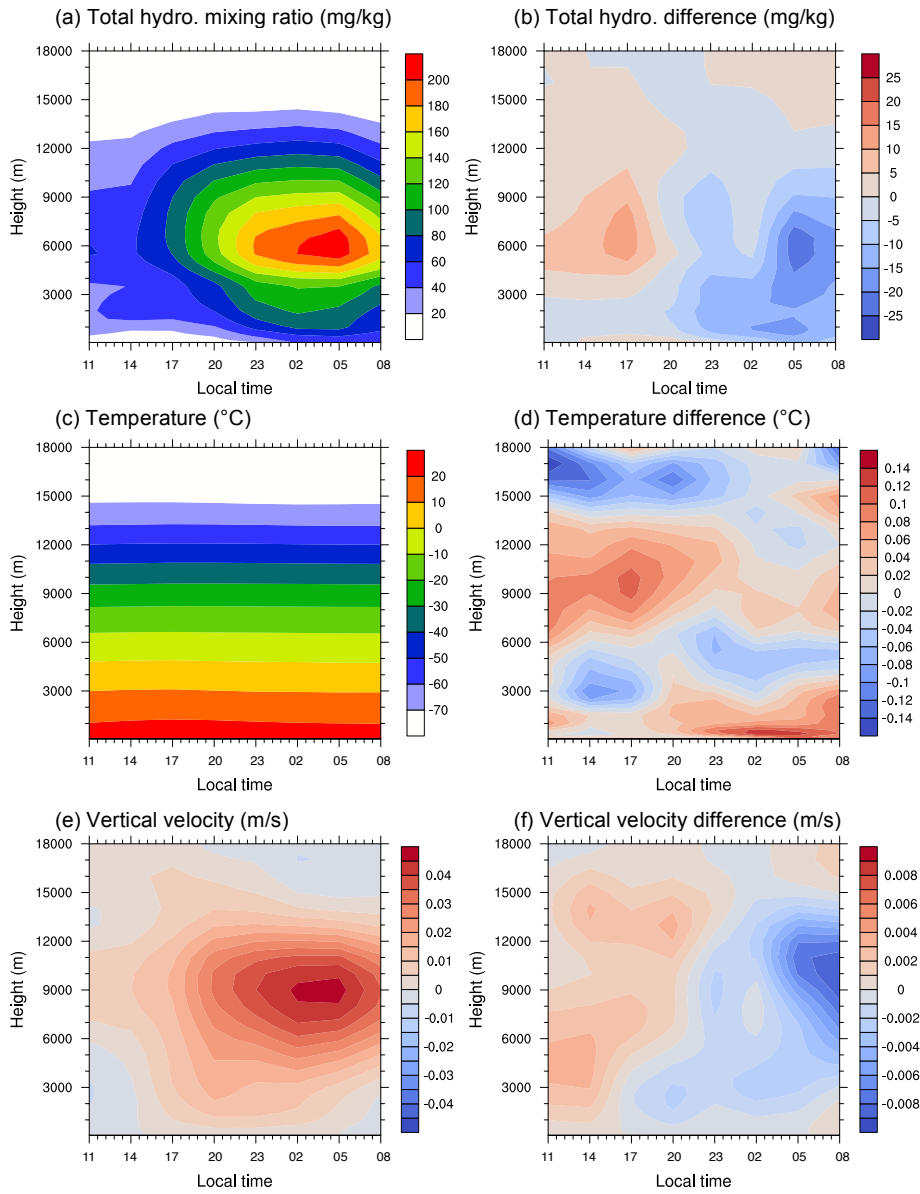
923
924

925
926

927
928 Figure 12. Diurnal evolution of vertical profiles over the Borneo region (r2) in FF for (a)
929 total hydrometeor mixing ratio (mg kg^{-1}), (c) temperature (°C), and (e) vertical velocity (m s[-
930 1]). Data are averaged all the nocturnal convections. (b), (d), and (f) is the differences
931 between FF and FFBB (FFBB-FF) for each parameter.

932

49

933

(a) Daytime – No fire

rainfall +
hydrometeors +

(b) Daytime – Fire event

Sea breeze

Sea breeze +

(c) Nighttime – No fire

(d) Nighttime – Fire event

Monsoon   Land breeze
Anticyclonic circulation

rainfall -
hydrometeors -

Monsoon   Land breeze -
Anticyclonic circulation

934
935   Figure 13. Schematics of diurnal rainfall/convection activity over the western Borneo. (a)
936   and (b) illustrate the formation of convection during the daytime without and with fire event,
937   respectively. (c) and (d) are the same as (a) and (b) but in the nighttime.

938

50